

Interface nano-confined acoustic waves in polymeric surface phononic crystals

Marco Travaglini, Damiano Nardi, Claudio Giannetti, Vitalyi Gusev, Pasqualantonio Pingue, Vincenzo Piazza, Gabriele Ferrini, and Francesco Banfi

Citation: [Applied Physics Letters](#) **106**, 021906 (2015); doi: 10.1063/1.4905850

View online: <http://dx.doi.org/10.1063/1.4905850>

View Table of Contents: <http://scitation.aip.org/content/aip/journal/apl/106/2?ver=pdfcov>

Published by the [AIP Publishing](#)

Articles you may be interested in

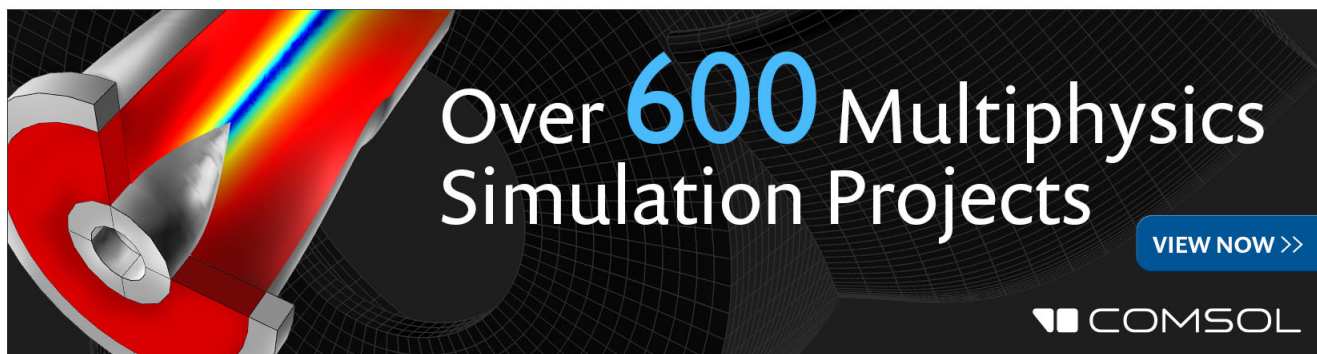
[Simulations of acoustic waves bandgaps in a surface of silicon with a periodic hole structure in a thin nickel film](#)
AIP Advances **4**, 077138 (2014); 10.1063/1.4892076

[Hypersonic phonon propagation in one-dimensional surface phononic crystal](#)
Appl. Phys. Lett. **104**, 123108 (2014); 10.1063/1.4870045

[Phononic dispersion of a two-dimensional chessboard-patterned bicomponent array on a substrate](#)
Appl. Phys. Lett. **101**, 053102 (2012); 10.1063/1.4739950

[Experimental demonstration of surface acoustic waves in two-dimensional phononic crystals with fluid background](#)
J. Appl. Phys. **106**, 044512 (2009); 10.1063/1.3200964

[Surface and interface shear horizontal acoustic waves in piezoelectric superlattices](#)
J. Appl. Phys. **87**, 4507 (2000); 10.1063/1.373097

The advertisement features a 3D simulation of a mechanical part with a red-to-blue color gradient representing stress or temperature. The text 'Over 600 Multiphysics Simulation Projects' is prominently displayed in white and blue. A blue button with the text 'VIEW NOW >>' is located in the bottom right corner. The COMSOL logo is also present in the bottom right corner.

Over **600** Multiphysics Simulation Projects

[VIEW NOW >>](#)

COMSOL

Interface nano-confined acoustic waves in polymeric surface phononic crystals

Marco Travagliati,^{1,2,a)} Damiano Nardi,³ Claudio Giannetti,⁴ Vitaliy Gusev,⁵ Pasqualantonio Pingue,² Vincenzo Piazza,¹ Gabriele Ferrini,⁴ and Francesco Banfi^{4,b)}

¹Center for Nanotechnology Innovation@NEST, Istituto Italiano di Tecnologia, Piazza San Silvestro 12, 56127 Pisa, Italy

²NEST, Scuola Normale Superiore and Istituto Nanoscienze-CNR, Piazza San Silvestro 12, 56127 Pisa, Italy

³JILA and Department of Physics, University of Colorado, 440 UCB, Boulder, Colorado 80309, USA

⁴i-LAMP and Dipartimento di Matematica e Fisica, Università Cattolica del Sacro Cuore, Via Musei 41, 25121 Brescia, Italy

⁵LAUM, UMR-CNRS 6613, Université du Maine, av. O. Messiaen, 72085 Le Mans, France

(Received 25 November 2014; accepted 31 December 2014; published online 14 January 2015)

The impulsive acoustic dynamics of soft polymeric surface phononic crystals is investigated here in the hypersonic frequency range by near-IR time-resolved optical diffraction. The acoustic response is analysed by means of wavelet spectral methods and finite element modeling. An unprecedented class of acoustic modes propagating within the polymer surface phononic crystal and confined within 100 nm of the nano-patterned interface is revealed. The present finding opens the path to an alternative paradigm for characterizing the mechanical properties of soft polymers at interfaces and for sensing schemes exploiting polymers as embedding materials. © 2015 Author(s). All article content, except where otherwise noted, is licensed under a Creative Commons Attribution 3.0 Unported License. [<http://dx.doi.org/10.1063/1.4905850>]

Elastic metamaterials are among the frontiers in materials science,^{1,2} paving the way to the era of nanophononics.^{3,4} Among them surface phononic crystals (SPCs) are metamaterials obtained by periodically nano-patterning the surface of a solid substrate, thus modulating the surface elastic properties. SPCs play a key role in technological applications due to their capability to sustain surface acoustic waves (SAWs)—mechanical oscillations confined within an acoustic wavelength λ from the surface—at the core of a variety of sensing schemes,^{5,6} opto-acoustics,⁷ and microfluidics devices.^{8–10} Excitation of hypersonic frequency SAWs in SPCs has been achieved by means of time-resolved all-optical techniques,^{11–15} lately reaching SAW confinements of few tens of nm.^{16–19} In this regime, SAW-generation in optically excited SPCs has been recently applied to the characterization of the elastic properties of hard thin-films¹⁹ and to alternative mass-sensing schemes, enabling superior sensitivities.²⁰ In order to widen the spectrum of applications, excitation of interface confined acoustic modes in SPCs made of soft materials is envisaged.

The present work investigates a composite polymer SPC/Al-Si SPC metamaterial. The Al-Si SPC is made of a periodic array of aluminum nanodisks having a diameter $d=350$ nm and a height $h=85$ nm deposited on a silicon(100) substrate with a pitch $P=1$ μ m. The Al-Si SPC is then coated with polydimethylsiloxane (PDMS), a soft and transparent polymer commonly used in SAW vapor sensors. PDMS molds to the Al-Si SPC through conformal-bonding, creating a polymeric overlay resembling a negative stamp of the Al-Si SPC: the polymeric overlay is thus a PDMS SPC (PDMS-SPC) and the composite PDMS-SPC plus Al-Si SPC

is addressed as polymer-coated SPC (p-SPC), as illustrated in Figure 1.

The impulsive acoustic dynamics of the soft PDMS-SPC adhering to the standard Al-Si SPC is here investigated and represents the focus of the paper, while the Al-Si SPC, in conjunction with ultra-short laser pulses, merely serves as an opto-acoustic (acousto-optic) transducer to trigger (detect) the interface confined oscillations in the soft polymer SPC. The simultaneous photo-acoustic excitation of interface nano-confined acoustic waves in the polymer, as well as conventional SAW Rayleigh-like modes confined in the Al-Si SPC, is demonstrated. The conventional Al-Si SPC modes are attenuated by the presence of the soft polymer overlay constituting the PDMS-SPC. The PDMS-SPC modes, on the other hand, arise from the nano-imprinting of the overlay surface created by the stiffer Al-Si SPC and exhibit a confinement on a length scale much tighter than the periodicity P , as it would be for standard SAW-like modes.²¹ These modes are distinctive of the PDMS-SPC, opening the path to an alternative paradigm for probing the mechanical properties of soft polymers at interfaces and for sensing schemes exploiting polymers as embedding materials. In this context, information are conventionally retrieved from modifications in the propagation dynamics of surface-confined acoustic modes pertaining to the substrate material (i.e., the Al-Si SPC), not by direct inspection of surface-confined oscillations within the polymer itself (i.e., the PDMS-SPC). The present findings bear great practical interest; mechanical characterisation of thin polymer films and interfaces is yet an important challenge in materials science, of relevance to nanoelectronics, nanomanufacturing, and biotechnology applications. For instance, in gas and biomolecules sensing technology, polymeric matrices are the go-to materials to capture the molecules to be analysed.²²

^{a)}Electronic mail: marco.travagliati@iit.it

^{b)}Electronic mail: francesco.banfi@unicatt.it



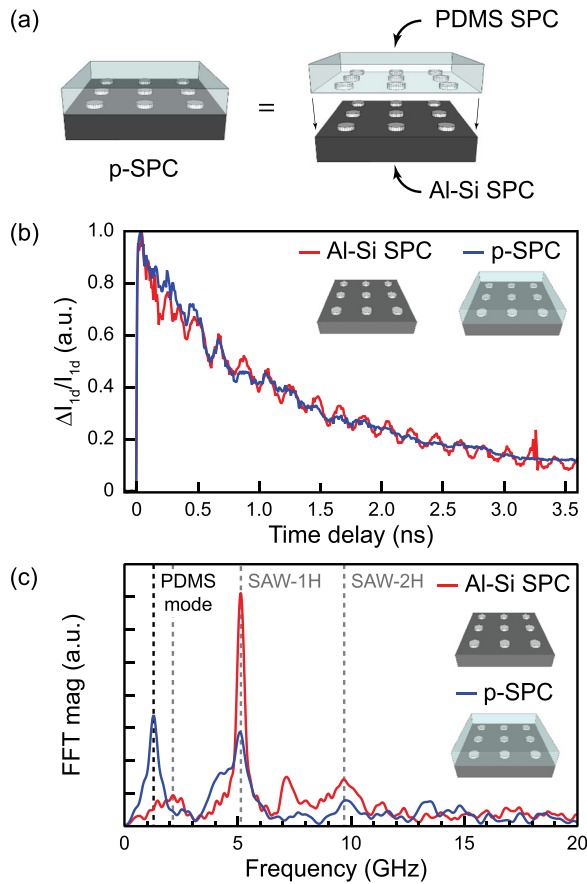


FIG. 1. (a) Schematics of the p-SPC as a composite of the PDMS-SPC and the Al-Si SPC. (b) Normalized relative variation of the diffracted signals for Al-Si SPC (red line) and p-SPC (blue line). (c) FFT magnitude obtained from the signals after subtraction of the thermal background. The fundamental and second pseudo-SAW harmonics of the Al-Si SPC are evidenced together with a broad shallow resonance peaked at 2.3 GHz (gray dashed lines). The PDMS confined mode at the 1.3 GHz is highlighted with the black dashed line.

Time-resolved measurements are performed by exciting the sample with an 800 nm wavelength, 120 fs laser pump pulse from a conventional Ti:sapphire oscillator. The absorbed energy density is peaked in the Al nanodisks leading to a temperature increase $dT \sim 2$ K within a few picoseconds. Energy is then dissipated via mechanical and thermal channels.²³ The thermal expansion of the Al disks generates a periodic displacement field $\mathbf{u}(\mathbf{r}, t)$. Among the complete set of eigenmodes $\{\mathbf{u}_i(\mathbf{r})\}$, solutions of the acoustic eigenvalue problem for the entire SPC (both in the case of the Al-Si SPC as well as the p-SPC), the experimental geometry and radial thermal expansion only allow for the excitation of modes at the center of the surface Brillouin zone with radial spatial symmetry. These are the only modes contributing to $\mathbf{u}(\mathbf{r}, t)$.

In the detection stage, the SPC doubles as an optical diffraction grating for a second time-delayed laser probe pulse. The relative variation of the probe diffracted intensity signal $\Delta I_{1d}/I_{1d}$ is modulated by the change in the surface optical form factor of the SPC driven by the excited eigenmodes. The signal is acquired from the first order diffraction spot to improve sensitivity with respect to standard reflectivity measurements.¹¹ The detection scheme is most sensitive to excited modes with a surface-confined (Al-Si SPC) or interface-confined (p-SPC) displacement field. Within the

thermal transport channel, the nanodisks' thermal expansion reverts as heat is dissipated to the substrate, contributing to a monotonically decreasing background in the $\Delta I_{1d}/I_{1d}$ signal.

The experimental traces for both the uncoated Al-Si SPC (red line) and p-SPC (blue line) are reported in Figure 1(b). The corresponding Fast Fourier Transform (FFT) spectra, calculated after subtraction of the monotonically decreasing thermal background, are shown in Figure 1(c). The Al-Si SPC oscillates at the fundamental (1H), 5.1 GHz, and second harmonic, 9.7 GHz, pseudo-SAW frequencies. The FFT peak at 7.1 GHz is identified as a bulk Al-Si SPC mode with a strong surface confinement, as the broad-low magnitude resonance peaked at 2.3 GHz. These modes have been discussed in detail by Nardi *et al.*¹¹ for the uncoated Al-Si SPC case with disks height $h = 45$ nm. In the p-SPC, the above-mentioned modes are attenuated, whereas a conspicuous portion of the spectral weight is transferred to a new peak at 1.29 GHz, the main *objective* of the present paper. Substituting $f = 1.29 \pm 0.28$ GHz and $\lambda = P = 1 \mu\text{m}$ (as required for the first mode at the center of the surface Brillouin zone) in the acoustic dispersion relation $c = f\lambda$, a value for the acoustic velocity $c = 1290 \pm 280$ m/s is found. This is consistent with values reported for longitudinal acoustic wave velocities for PDMS in the hypersonic frequency range.^{24–26} These results are robust and independent from fabrication details, being the same in both the case of conformal-bonded and spin-coated PDMS-SPCs.²¹ The emerging scenario for the main p-SPC resonance at 1.29 GHz is that of an acoustic wave (1) characterized by a strong interface confinement, (2) with an acoustic wavelength dictated by the PDMS-SPC periodicity, (3) living in the PDMS-SPC, and (4) longitudinally polarized in proximity of the interface, the acoustic wave propagation being assumed parallel to the interface as expected for an interface-confined mode. This point, although consistent with experimental findings, will find a stringent proof in the finite element modeling (FEM) addressed further on in the manuscript.

In order to gain further insight in the acoustic dynamics of the p-SPC in terms of modal analysis and excited mode lifetimes, with particular reference to the 1.29 GHz resonance, we implement a Wavelet Transform (WT) analysis. The WT projects the time-dependent signal $\Delta I_{1d}/I_{1d}$ over a time-frequency basis set. A time-frequency representation of the signal is thus obtained, each time-frequency coordinate being defined within a Heisenberg uncertainty box.

Figures 2(a) and 2(b) show the WT spectrum for the Al-Si SPC and p-SPC, respectively. In the Al-Si SPC, the 1H pseudo-SAW mode at 5.1 GHz persists within the entire 3.5 ns window explored in this experiment, whereas the other modes identified by the FFT are comparatively short-lived. In the p-SPC, the amplitudes and lifetimes of the above-addressed resonances are reduced, since energy is allocated to the 1.29 GHz excited mode. We model the $\Delta I_{1d}/I_{1d}$ signal as a sum of damped harmonic oscillators and retrieve the amplitudes, frequencies, and lifetimes from the WT spectrum following the procedure outlined by Pukhova *et al.*²⁷ In the p-SPC, the lifetime of the 1H pseudo-SAW is reduced from 5.5 ns of the uncoated Al-Si SPC to 600 ps, whereas the lifetime of the p-SPC 1.29 GHz resonance is 1.5 ns. As to the

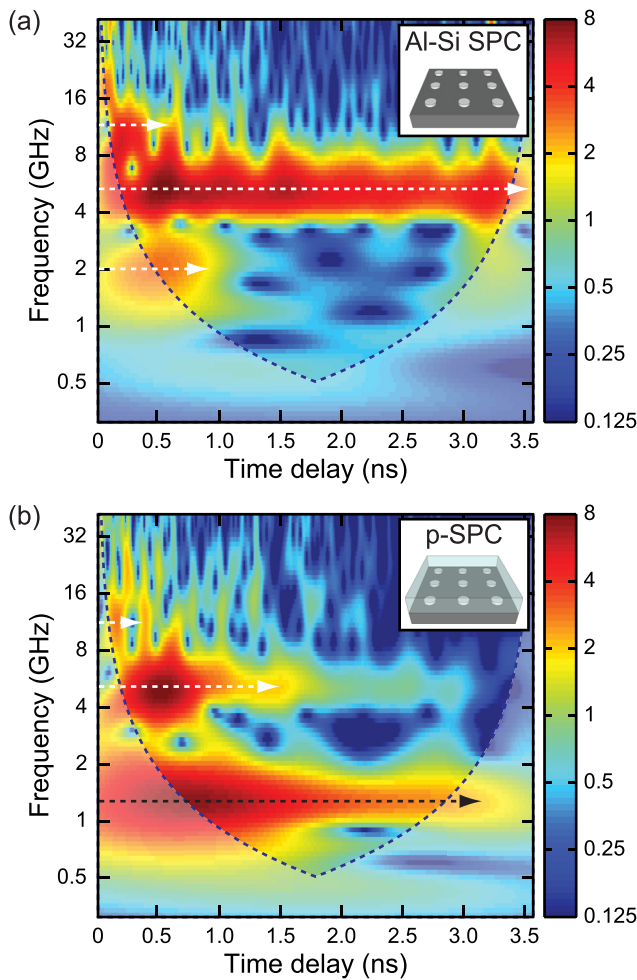


FIG. 2. Wavelet transform magnitude obtained from the experimental signal of Figure 1(b) after subtraction of the thermal background for (a) the Al-Si SPC case and (b) the p-SPC case. Shaded areas indicate points in time-frequency space where the wavelet spectral analysis is unreliable due to edge artifacts. The color scale is represented in octaves. Dashed arrows highlight the same resonances addressed in Figure 1(c).

origin of the 1.29 GHz resonance, modal down-conversion can be ruled-out. If this were the case, one would expect the 1.29 GHz oscillation to start at a time where the 1H pseudo-SAW mode signal diminishes. On the same basis, intramodal conversion from the low frequency tail of the broad Al-Si SPC resonance peaked at 2.3 GHz to the 1.29 GHz

resonance may also be excluded. In fact, WT analysis suggests that the 1.29 GHz resonance is launched directly in the PDMS-SPC overlay rather than being generated by a mode-conversion process involving the Al-Si SPC modes.

The scenario emerging from the measurement is rationalized via FEM. In the Al-Si SPC, the radial expansion of the disks excites several modes around 1.29 GHz, entering the broad resonance peaked at 2.3 GHz. These modes can trigger a surface-confined acoustic oscillation in the PDMS-SPC at 1.29 GHz and of radial spatial symmetry. The strategy is to solve the acoustic eigenvalue problem for the PDMS-SPC overlay to reproduce the displacement field and investigate the existence of modes bearing the above-mentioned characteristics, hence prone to being launched by the radial expansion of the disks.

The problem is simplified by modeling the PDMS as a non-viscous fluid, hence sustaining only longitudinal acoustic waves.^{26,28} This assumption is also suggested by the experimental findings, evoking a longitudinal polarization for the 1.29 GHz resonance. To reduce the computational complexity to a manageable size, the model is downscaled to a 2D geometry, considering the cross-section of the 3D unit cell, as shown in Figure 3(a). Nardi *et al.* demonstrated that the acoustic eigenspectra of 1D-SPCs (2D geometry) and 2D-SPCs (3D geometry) show similar features, thus providing support to the present simplification.¹¹ The eigenvalue problem for the pressure field p in the PDMS-SPC then reads: $\nabla^2 p + (\omega^2/c^2)p = 0$, with $c = 1290$ m/s as the acoustic velocity deduced from the measurements, ω as the angular frequency, and p as the pressure field. With reference to the unit cell of the PDMS-SPC depicted in Figure 3(a), Born-Von Karman periodic boundary conditions are implemented on the cell's lateral boundaries. Soft-wall boundary conditions, $p = 0$, apply to the top PDMS free surface. The Al-Si SPC is much stiffer than the PDMS-SPC, the Young's modulus being 70 GPa for Al, 126 GPa for Si, and in the 300–800 kPa range for PDMS. For this reason, the boundary conditions $\nabla p \cdot \mathbf{n} = 0$ are enforced at the PDMS-SPC/Al-Si SPC interface.

Once the eigenvalue equation for the pressure field is solved via FEM, the displacement field in Fourier space is retrieved by $\mathbf{U}_f = 1/[(2\pi f)^2 \rho_0] \nabla P_f$, where ρ_0 is the unperturbed PDMS density, $\mathbf{U}_f = \mathbf{F}\{u_f\}$ and $P_f = \mathbf{F}\{p_f\}$, $\mathbf{F}\{\cdot\}$,

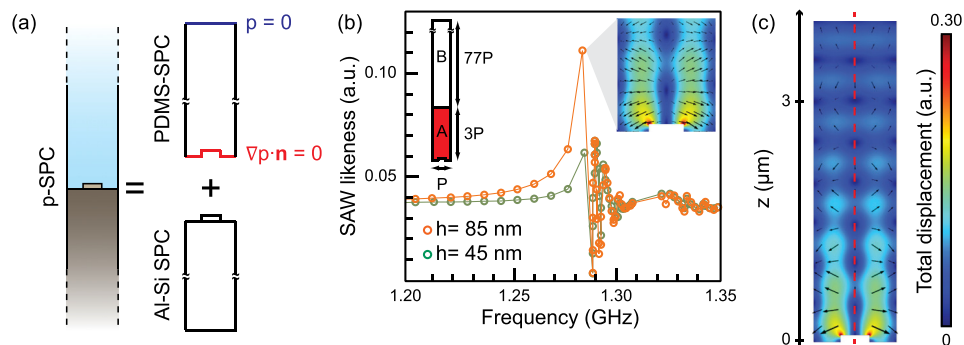


FIG. 3. (a) Schematics of the unit cell and boundary conditions. (b) SAW-likeness coefficient of the symmetric PDMS-SPC eigenmodes for disk height of 85 nm (orange circles) and 45 nm (green circles). Left inset: integration domain adopted for the calculation of the SAW-likeness coefficient. Right inset: details of the displacement field of the eigenmode f_{res} with the highest SAW-likeness coefficient. (c) Displacement field of the eigenmode f_{res} reported up to a unit cell's height of 4 μm . The color scale ranges up to 30% of the maximum displacement, which is located at the corners of the PDMS indentations, resulting in a saturation helping the visualization.

indicating the Fourier Transform operator. In order to spot out the solutions characterized by an interface-confined displacement field in the PDMS-SPC, the SAW-likeness coefficient $\alpha(f)$ is calculated for each eigenmode.²⁹ The SAW-likeness coefficient identifies eigenmodes with mechanical energy confined in close proximity of the interface. The calculation is here performed taking $\alpha(f) = \langle E_A(f) \rangle / \langle E_{\text{tot}}(f) \rangle$, with $\langle E_A(f) \rangle$ and $\langle E_{\text{tot}}(f) \rangle$ being the time-averaged mechanical energy contents of the eigenmode at frequency f in domain A and in the entire PDMS-SPC unit cell, respectively, as illustrated in the inset of Figure 3(b). Figure 3 reports $\alpha(f)$ calculated for even-symmetry eigenmodes, the only ones susceptible of being launched.³⁰ A resonance stands out at $f_{\text{res}} = 1.29$ GHz, matching the experimental value. The corresponding displacement field, illustrated in Figure 3(c) up to a distance of $4 \mu\text{m}$ from the interface and detailed in the inset of Figure 3(b) over a smaller scale, shows a strong surface confinement, dropping to 20% of its maximum value within the first 100 nm from the interface with the Al-Si SPC. The displacement within the first $1.5 \mu\text{m}$ from the interface is oriented predominantly parallel to the interface. This mode is due to the nano-imprinting of the PDMS surface: as the indentation's height h is reduced, $\alpha(f_{\text{res}})$ diminishes accordingly, f_{res} remaining substantially unaltered. This is shown in Figure 3(b) comparing $\alpha(f)$ for the cases $h = 45$ nm and $h = 85$ nm. As to the effect of periodicity, the value f_{res} was found to correctly scales as $1/P$, downshifting to 0.647 GHz for $P = 2 \mu\text{m}$. These evidences rationalize the experimental findings. In a perturbative step-like view, the laser-driven thermal expansion of the disks launches surface-confined Al-Si SPC eigenmodes among which the broad resonance peaked at 2.3 GHz overlaps the PDMS-SPC resonance at 1.29 GHz. In these breathing modes of the disks, the expansion is predominantly radial. The disks lateral boundaries motion compresses the adhering PDMS. The PDMS compression profile triggers the PDMS-SPC 1.29 GHz-eigenmode displacement profile in close proximity to the disks, as shown in the insets of Figures 3(b) and 3(c). The acoustic-wave modulating the optical-diffraction grating at 1.29 GHz is thus longitudinally polarized parallel to the interface. Accounting for the p-SPC as a whole, the synopsis of the dynamics is the following: the initial heat-driven displacement field launches a p-SPC eigenmode that, on the polymer side of the interface, resembles the PDMS-SPC eigenmode theoretically addressed above. This eigenmode ultimately drives the unit cell's optical form factor at its characteristic frequency, hence modulating the optical signal at 1.29 GHz.

It is worth mentioning that, if one considers PDMS as a fluid, Scholte waves should be considered as a potential mechanism accounting for the observed signal. However, in the present case, Scholte waves can be ruled out as the dominant mechanism, even if they may occur at a similar frequency. In fact, the decay length of a Scholte wave²¹ on the PDMS side is $\sim 20P$, which is $20 \mu\text{m}$ in the current configuration. The initial displacement triggered by the disks radial expansion is therefore much more effective in launching the 100 nm confined acoustic oscillation arising from the PDMS nano-imprinting.

In conclusion, the full thermo-mechanics of a composite polymer-solid phononic crystal operating in the hypersonic frequency range has been investigated. Photoacoustic excitation and characterization of an unprecedented class of interface-confined acoustic modes on the PDMS-SPC side of the interface has been shown. The origin of these modes is from polymer surface nano-imprinting. The interface confinement in the polymer is extremely tight, dropping to 20% of its maximum value within the first 100 nm from the interface with the Al-Si SPC, which is approximately $P/10$, one order of magnitude tighter with respect to the confinement P of standard SAW modes. The penetration depth within the polymer can be tuned by controlling the phononic crystals indentation height and periodicity. The present findings are of relevance in view of applications in fields ranging from acoustic nanometrology to polymer interface physics and acoustic wave-based sensing. Furthermore, the concept is readily transferable to solid-fluid phononic crystals,³¹ hence directly integrable in microfluidics device architectures.

F.B. acknowledges financial support by the MIUR-“Futuro in ricerca 2013” Grant in the frame of the ULTRANANO Project and Università Cattolica through D.2.2 and D.3.1 funding. The authors acknowledge Dr. Marco Cecchini for the support provided in PDMS processing.

- ¹J.-H. Lee, J. P. Singer, and E. L. Thomas, *Adv. Mater.* **24**, 4782 (2012).
- ²M. Wegner, *Science* **22**, 939 (2013).
- ³J.-W. Lee, C. Y. Koh, J. P. Singer, S. J. Jeon, M. Maldovan, O. Stein, and E. L. Thomas, *Adv. Mater.* **26**, 532 (2014).
- ⁴M. Maldovan, *Nature* **503**, 209 (2013).
- ⁵P. Hess, *Phys. Today* **55**(3), 42 (2002).
- ⁶T. M. A. Gronewold, *Anal. Chim. Acta* **603**, 119 (2007).
- ⁷M. M. de Lima, Jr. and P. V. Santos, *Rep. Prog. Phys.* **68**, 1639 (2005).
- ⁸L. Y. Yeo and J. R. Friend, *Annu. Rev. Fluid Mech.* **46**, 379 (2014).
- ⁹Y. Bourquin, R. Wilson, Y. Zhang, J. Reboud, and J. M. Cooper, *Adv. Mater.* **23**, 1458 (2011).
- ¹⁰R. J. Shilton, M. Travagliati, F. Beltram, and M. Cecchini, *Adv. Mater.* **26**, 4941 (2014).
- ¹¹D. Nardi, M. Travagliati, M. E. Siemens, Q. Li, M. M. Murnane, H. C. Kapteyn, G. Ferrini, F. Parmigiani, and F. Banfi, *Nano Lett.* **11**, 4126 (2011).
- ¹²G. A. Antonelli, H. J. Maris, S. G. Malhotra, and J. M. E. Harper, *J. Appl. Phys.* **91**, 3261 (2002).
- ¹³R. I. Tobey, E. H. Gershgoren, M. E. Siemens, M. M. Murnane, H. C. Kapteyn, T. Feurer, and K. A. Nelson, *Appl. Phys. Lett.* **85**, 564 (2004).
- ¹⁴D. M. Profunser, O. B. Wright, and O. Matsuda, *Phys. Rev. Lett.* **97**, 055502 (2006).
- ¹⁵P. H. Otsuka, K. Nanri, O. Matsuda, M. Tomoda, D. M. Profunser, I. A. Veres, S. Danworaphong, A. Khelif, S. Benchabane, V. Laude, and O. B. Wright, *Sci. Rep.* **3**, 3351 (2013).
- ¹⁶M. E. Siemens, Q. Li, M. M. Murnane, H. C. Kapteyn, R. Yang, E. H. Anderson, and K. A. Nelson, *Appl. Phys. Lett.* **94**, 093103 (2009).
- ¹⁷Q. Li, K. Hoogeboom-Pot, D. Nardi, M. M. Murnane, H. C. Kapteyn, M. E. Siemens, E. H. Anderson, O. Hellwig, E. Dobisz, B. Gurney, R. Yang, and K. A. Nelson, *Phys. Rev. B* **85**, 195431 (2012).
- ¹⁸M. Schubert, M. Grossmann, O. Ristow, M. Hettich, A. Bruchhausen, E. C. S. Barretto, E. Scheer, V. Gusev, and T. Dekorsy, *Appl. Phys. Lett.* **101**, 013108 (2012).
- ¹⁹D. Nardi, K. M. Hoogeboom-Pot, J. N. Hernandez-Charpak, M. Tripp, S. W. King, E. H. Anderson, M. M. Murnane, and H. C. Kapteyn, *Proc. SPIE* **8681**, 86810N (2013).
- ²⁰D. Nardi, E. Zagato, G. Ferrini, C. Giannetti, and F. Banfi, *Appl. Phys. Lett.* **100**, 253106 (2012).
- ²¹See supplementary material at <http://dx.doi.org/10.1063/1.4905850> for the nanofabrication protocol, wavelet and FEM details, supplementary data on

- spin-coated devices, on $P=2\ \mu\text{m}$ device simulation, and Stoneley and Scholte wave calculation details.
- ²²J. W. Grate, *Chem. Rev.* **100**, 2627 (2000).
- ²³F. Banfi, F. Pressacco, B. Revaz, C. Giannetti, D. Nardi, G. Ferrini, and F. Parmigiani, *Phys. Rev. B* **81**, 155426 (2010).
- ²⁴M. Sinha, J. E. Mark, H. E. Jackson, and D. Walton, *J. Chem. Phys.* **117**, 2968 (2002).
- ²⁵J.-H. Jang, C. K. Ullal, T. Gorishnyy, V. V. Tsukruk, and E. L. Thomas, *Nano Lett.* **6**, 740 (2006).
- ²⁶J. Shi, S. Yazdi, S.-C. S. Lin, X. Ding, I.-K. Chiang, K. Sharp, and T. J. Huang, *Lab Chip* **11**, 2319 (2011).
- ²⁷V. Pukhova, F. Banfi, and G. Ferrini, *Nanotechnology* **24**, 505716 (2013).
- ²⁸S. Zhou, P. Reynolds, R. Krause, T. Buma, M. O'Donnell, and J. A. Hossack, *IEEE Trans. Ultrason. Ferroelectr. Freq. Control* **51**, 1178 (2004).
- ²⁹D. Nardi, F. Banfi, C. Giannetti, B. Revaz, G. Ferrini, and F. Parmigiani, *Phys. Rev. B* **80**, 104119 (2009).
- ³⁰The even symmetry is with respect to inversion versus the unit cell's vertical axis of symmetry: even-symmetry eigenmodes are the 2D analogue of radial symmetry eigenmodes in the 3D case.
- ³¹R. P. Moiseyenko, N. F. Declercq, and V. Laude, *J. Phys. D: Appl. Phys.* **46**, 365305 (2013).

Interface nano-confined acoustic waves in polymeric surface phononic crystals

Marco Travagliati,^{1,2, a)} Damiano Nardi,³ Claudio Giannetti,⁴ Vitalyi Gusev,⁵ Pasqualantonio Pingue,² Vincenzo Piazza,¹ Gabriele Ferrini,⁴ and Francesco Banfi^{4, b)}

¹⁾Center for Nanotechnology Innovation @ NEST, Istituto Italiano di Tecnologia, Piazza San Silvestro 12, 56127 Pisa, Italy

²⁾NEST, Scuola Normale Superiore and Istituto Nanoscienze-CNR, Piazza San Silvestro 12, 56127 Pisa, Italy

³⁾JILA and Department of Physics, University of Colorado, 440 UCB, Boulder, CO80309, Colorado, USA

⁴⁾i-LAMP and Dipartimento di Matematica e Fisica, Università Cattolica del Sacro Cuore, Via Musei 41, 25121 Brescia, Italy

⁵⁾LAUM, UMR-CNRS 6613, Université du Maine, av. O. Messiaen, 72085 Le Mans, France

I. SAMPLE NANOFABRICATION

The Al-Si SPCs have been fabricated by standard electron-beam lithography and lift off techniques. PDMS has been prepared using a Dow Corning Sylgard 184 kit. The precursor has been mixed 10:1 in weight with the curing agent, vacuum degassed and cross-linked for 15 minutes in an oven at 120° (further details are reported by Travagliati *et al.*)¹. The p-SPC has been obtained by molding the PDMS on top of the Al-Si SPC either by conformal-bonding or spin-coating. In the first case, the mix was cast on a bare silicon wafer prior to degassing to obtain a 1.4 mm thick PDMS layer. PDMS was peeled from the wafer after baking and manually deposited onto the Al-Si SPC surface. In the case of spin-coated p-SPC, the mix was spun at 10 000 rpm for 1 min on the Al-Si SPC prior to baking.

II. WAVELET ANALYSIS

Wavelet analysis is based on the projection (convolution) of the discrete time signal $\Delta I_{1d}/I_{1d}$, onto a set of continuous functions $\psi_{s,d}(t)$ —sisters wavelets—derived from translations and dilations of a Morlet mother wavelet

$$\psi(\omega, t) = (\pi\sigma^2)^{-1/4} \exp(-t^2/2\sigma^2) \exp(-i\omega t),$$

where σ controls the amplitude of the Gaussian envelope and consequently its time-frequency resolution (Heisenberg uncertainty box), and ω is the carrier angular frequency. The Gaussian envelope has here been chosen so as to allow for four oscillations of the daughter wavelets at any chosen frequency. Further details can be found in previous works²⁻⁴.

III. THEORETICAL MODELING

FEM calculations have been implemented in COMSOL Multiphysics 4.2a and run on an Intel mainframe (24 CPUs and 256 GB of RAM). The modeled geometry consists of a single unit cell of the PDMS-SPC having a width of $P = 1 \mu\text{m}$. Periodic boundary conditions have been applied on the sides of the unit cell to reproduce the entire phononic crystal geometry. In order to achieve a high enough density of eigenmodes to finely reproduce their frequency spectrum, i.e. to spot out the interface-confined resonance, the solution of the acoustic eigenvalue problem has been calculated on an unit cell having an height of 80 μm . The simulation cell has been divided into three layers of different mesh elements density. The first fine-meshed layer starts at the nanostructured interface and has a thickness of $2h$, h being the nano-indentation height. The maximum mesh element size is $P/628$. The second layer, of intermediate mesh density, extends from the top of the first layer up to a quote of $3P$ within the PDMS overlay. Here, the maximum mesh element size is $P/128$. The third coarse-meshed layer includes the remaining portion of the PDMS overlay. The maximum mesh element size here is $P/32$. Numerical codes have been implemented in MATLAB and JAVA to post-process the FEM simulation results.

IV. STONELEY AND SCHOLTE WAVES

We now show that Stoneley waves are not supported at the flat silicon-PDMS interface.

The equation for the speed of Stoneley waves c reads⁵:

^{a)}Electronic mail: marco.travagliati@iit.it

^{b)}Electronic mail: francesco.banfi@unicatt.it

$$\Delta(c) = \begin{vmatrix} 1 & 1 & -1 & -1 \\ \frac{b_1}{k} & \frac{k}{b_2} & \frac{b_3}{k} & \frac{k}{b_4} \\ \frac{2b_1}{k} & \left(2 - \frac{c^2}{\beta_1^2}\right) \frac{k}{b_2} & \frac{2\mu_2}{\mu_1} \frac{b_3}{k} & \frac{2\mu_2}{\mu_1} \left(2 - \frac{c^2}{\beta_1^2}\right) \frac{k}{b_4} \\ 2 - \frac{c^2}{\beta_1^2} & 2 & -\frac{\mu_2}{\mu_1} \left(2 - \frac{c^2}{\beta_2^2}\right) & -2\frac{\mu_2}{\mu_1} \end{vmatrix} = 0 \quad (1)$$

where the subscript 1 and 2 refer to the two different solids, α is the longitudinal speed of sound, β the transverse speed of sound, ρ the mass density, $\mu = \rho\beta^2$ the rigidity, ω the angular frequency, $k = \omega/c$, and

$$\begin{aligned} b_1 &= k \left(1 - \frac{c^2}{\alpha_1^2}\right)^{\frac{1}{2}}, \\ b_2 &= k \left(1 - \frac{c^2}{\beta_1^2}\right)^{\frac{1}{2}}, \\ b_3 &= k \left(1 - \frac{c^2}{\alpha_2^2}\right)^{\frac{1}{2}}, \\ b_4 &= k \left(1 - \frac{c^2}{\beta_2^2}\right)^{\frac{1}{2}}. \end{aligned}$$

In our system we have for silicon $\rho_1 = 2329 \text{ kg/m}^3$, $\alpha_1 = 8430 \text{ m/s}$, and $\beta_1 = 5840 \text{ m/s}$, as measured by Yurtsever and Zewail⁶ in Si[100]. For PDMS, we considered $\rho_2 = 965 \text{ kg/m}^3$, $\alpha_2 = 1290 \text{ m/s}$ and $\beta_2 = 500 \text{ m/s}$, where

the transverse speed of sound was taken from Zhu *et al.*⁷.

Figure S3 reports the real and imaginary part of $\Delta(c)$. In order for a Stoneley wave solution to exist, $\Delta(c)$ must be zero for a positive real value of c . Figure S3 shows that, for our material parameters, this condition cannot be met. We therefore rule out the existence of Stoneley waves in our system.

For sake of completeness, we now show, that, if we instead consider cross-linked PDMS acoustically as a fluid^{8–10}, although a Scholte wave solution exists at the interface between flat PDMS and silicon, it may be ruled out as the leading mechanism responsible for the observed peak at 1.29 GHz in our measurement.

The speed of Scholte waves can be obtained from the Equation 1 in the limit $\beta_2 \rightarrow 0$, thus reading

$$\Delta(c) = \begin{vmatrix} 1 & 1 & -1 & -1 \\ \frac{b_1}{k} & \frac{k}{b_2} & \frac{b_3}{k} & 0 \\ \frac{2b_1}{k} & \left(2 - \frac{c^2}{\beta_1^2}\right) \frac{k}{b_2} & 0 & 0 \\ 2 - \frac{c^2}{\beta_1^2} & 2 & \frac{\rho_2 c^2}{\mu_1} & 0 \end{vmatrix} = 0$$

Following the same steps as for the case of Stoneley waves, a solution is found for $c \sim \alpha_2$, as expected from the literature¹¹. Nevertheless, the Scholte wave can be excluded as the leading mechanism responsible for the detected signal on the basis of its penetration depth. The penetration depth is given by the formula¹¹

$$L_{\text{Scholte}} = \frac{\lambda \rho_1 (\alpha_1^2 - \beta_1^2)}{\pi \rho_2 \alpha_2^2}.$$

For our material combination we obtain $L_{\text{Scholte}} \sim 20\lambda = 20P$, that is ~ 200 times greater than the penetration depth of the mode arising from the nano-imprinting of the PDMS. For this reason, as detailed in the main text, the launching efficiency of the former is negligible compared to the launching efficiency of the latter.

REFERENCES

- ¹M. Travaglini, R. Shilton, F. Beltram, and M. Cecchini, *J. Visualized Exp.* **78**, e50524 (2013).
- ²V. Pukhova, F. Banfi, and G. Ferrini, *Nanotechnology* **24**, 505716 (2013).
- ³F. Banfi and G. Ferrini, *Beilstein J. Nanotechnol.* **3**, 294 (2012).
- ⁴V. Pukhova, F. Banfi, and G. Ferrini, *Beilstein J. Nanotechnol.* **5**, 494 (2014).
- ⁵J. Achenbach, *Wave propagation in elastic solids* (Elsevier, 1984).
- ⁶A. Yurtsever and A. H. Zewail, *Proc. Natl. Acad. Sci. U. S. A.* **108**, 3152 (2011).
- ⁷G. Zhu, N. Z. Swintek, S. Wu, J. S. Zhang, H. Pan, J. D. Bass, P. A. Deymier, D. Banerjee, and K. Yano, *Phys. Rev. B* **88**, 144307 (2013).
- ⁸J. Shi, S. Yazdi, S.-C. S. Lin, X. Ding, I.-K. Chiang, K. Sharp, and T. J. Huang, *Lab Chip* **11**, 2319 (2011).
- ⁹M. Sinha, J. E. Mark, H. E. Jackson, and D. Walton, *J. Chem. Phys.* **117**, 2968 (2002).
- ¹⁰L. L. Stevens, E. B. Orlor, D. M. Dattelbaum, M. Ahart, and R. J. Hemley, *J. Chem. Phys.* **127**, 104906 (2007).
- ¹¹J. D. N. Cheeke, *Fundamentals and applications of ultrasonic waves* (CRC Press, 2012).

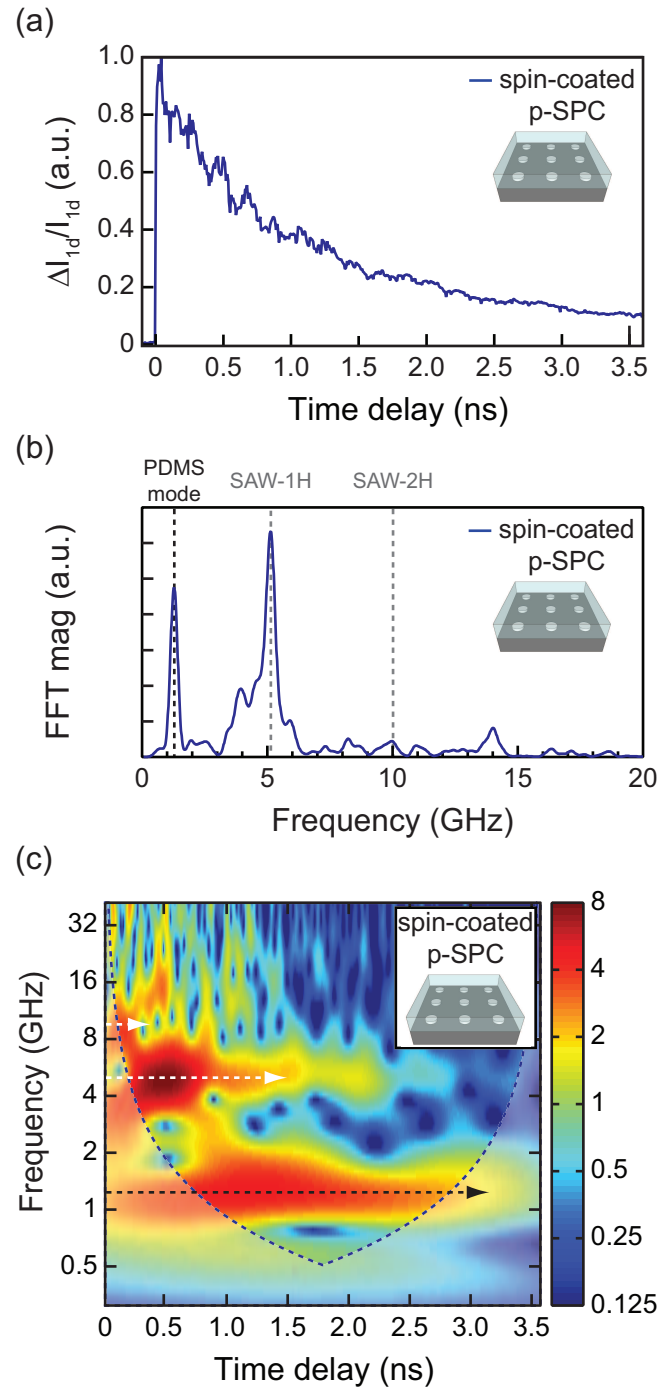


FIG. S1. (a) Normalized relative variation of the diffracted signals measured in the transient near-IR diffraction experiment on the p-SPC obtained through PDMS spin-coating. (b) FFT magnitude obtained from the signals in the top panel after subtraction of the thermal background. Dashed lines highlight the same resonances observed in Figure 1 of the main text. (c) WT magnitude obtained from the experimental signal on the spin-coated p-SPC after subtraction of the monotonically decreasing thermal background. Shaded areas indicate points in time-frequency space where the wavelet spectral analysis is unreliable due to edge artifacts. The color scales are represented in octaves. Dashed arrows highlight the same resonances addressed in panel (b). Insets: schematics of the SPCs under investigation.

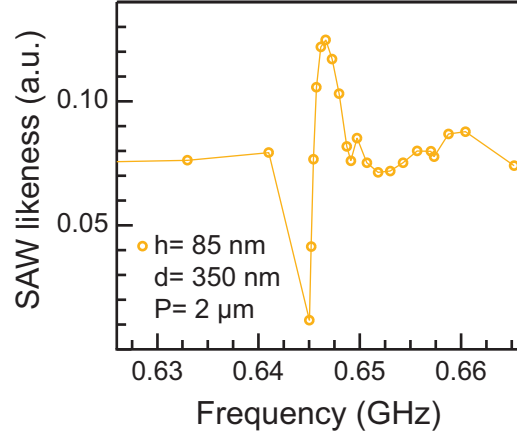


FIG. S2. Symmetric eigenmodes SAW-likeness coefficient for a PDMS-SPC with $h = 85$ nm, $d = 350$ nm and $P = 2$ μ m.

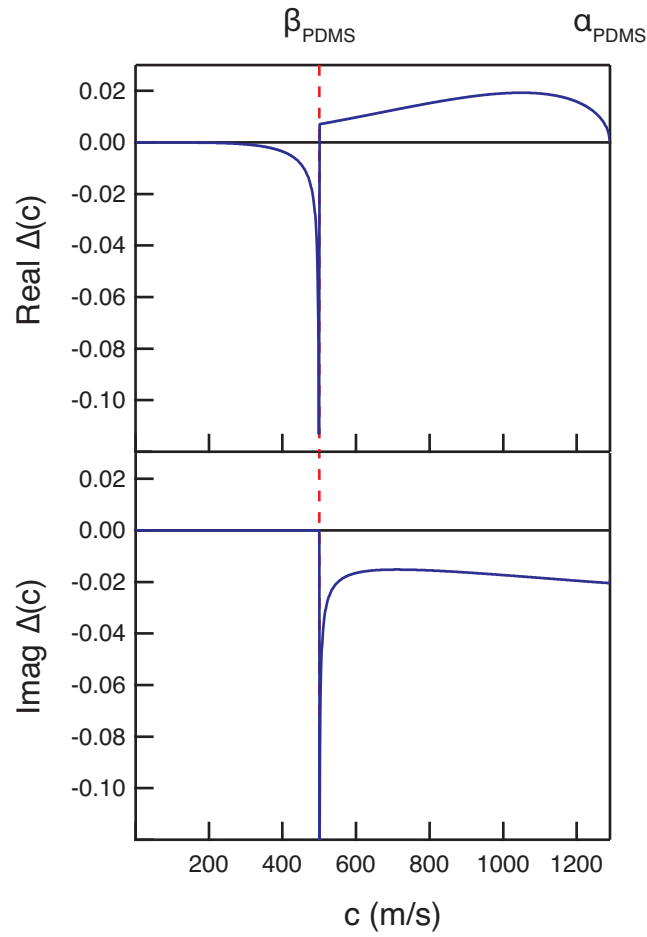


FIG. S3. Real and imaginary part of $\Delta(c)$ at the silicon-PDMS interface as a function of the hypothetical Stoneley wave speed c .